Corrected 28 April 2023. See full text.

OPTICAL FIBERS

Scaling information pathways in optical fibers by topological confinement

Zelin Ma[1], Poul Kristensen[2], Siddharth Ramachandran[1]*

Spatial mode-count scalability in optical fibers is of paramount importance for addressing the upcoming information-capacity crunch, reducing energy consumption per bit, and for enabling advanced quantum computing networks, but this scalability is severely limited by perturbative mode mixing. We show an alternative means of light guidance, in which light's orbital angular momentum creates a centrifugal barrier for itself, thereby enabling low-loss transmission of light in a conventionally forbidden regime wherein the mode mixing can be naturally curtailed. This enables kilometer-length-scale transmission of a record ~50 low-loss modes with cross-talk as low as −45 decibels/kilometer and mode areas of ~800 square micrometers over a 130-nanometer telecommunications spectral window. This distinctive light-guidance regime promises to substantially increase the information content per photon for quantum or classical networks.

Light transport with optical fibers in multiple orthogonal dimensions of a photon is of great utility for increasing the information capacity of classical communications networks, reducing energy consumption per bit, as well as for facilitating development of advanced quantum computing networks in high-dimensional Hilbert spaces (*1*, *2*). With degrees of freedom such as wavelength, amplitude, phase, and polarization having been exhausted, spatial multiplexing remains the last available dimension to be considered (*3*). Two primary approaches for exploiting space comprise the use of multimode fibers (MMFs), whose spatial modes are mutually orthogonal, and multicore fibers (MCFs), which consist of multiple single-mode waveguide cores. MCFs are appealing, given their deployment simplicity and backward compatibility, but their individual cores must be sufficiently spatially separated to avoid cross-talk, a requirement that limits channel-count scalability because reliability considerations place an upper limit on overall fiber dimensions (*3*). MMFs, by contrast, feature several benefits, such as high spatial efficiency—because all spatial modes occupy the same waveguiding core—and cost and efficiency savings through shared-pump optical amplification (*4*). However, modes in conventional MMFs stochastically couple with each other because of ever-present ambient perturbations, a problem that can be addressed through the use of multi-input–multi-output digital signal processing (MIMO-DSP) in classical communications systems (*3*), wherein mode mixing may actually be preferred. But this necessarily increases the complexity and power consumption of the receiver, and, crucially, this solution cannot be applied to single photons in quantum networks. An ideal solution would be an MMF whose modes behave like the separated cores of an MCF, because it would deliver the benefits of both approaches. However, MMFs designed to limit mode mixing over kilometer-length scales have achieved only up to 12 modes (*5*), and even so, with cross-talk considerably worse than those of MCFs. Further scalability has eluded the scientific community for almost a decade.

Here, we demonstrate a mechanism to transmit light over long lengths of optical fibers by exploiting a topological effect wherein the photon remains confined to a fiber as a result of a centrifugal barrier that light's orbital angular momentum (OAM) creates for itself. This form of light guidance is forbidden by the principles of total internal reflection (TIR), the primary means for light transport demonstrated by Colladon, Babinet, and Tyndall more than 150 years ago. Not restricted by the TIR condition, this regime of light transport results in propagating eigenstates that are naturally immune to perturbative mode mixing. We validate the practical utility of these modes, hereafter called topologically confined modes (TCMs), by demonstrating light transmission over a record number of low-loss spatial modes with negligible mode coupling over a kilometer of fiber, featuring mode areas that are an order of magnitude greater than that available from single-mode fibers (SMFs) or MCFs, even when they are tightly bent. We show that these beneficial metrics can be obtained over multiple spectral bands in use for telecommunications today.

Concept and demonstration of topological confinement

A heuristic ray picture of the concept of topological confinement is shown in Fig. 1A (*6*). It schematically depicts a step-index fiber comprising a high-index core, n_{co}, surrounded by a low-index cladding, n_{cl}, and three exemplary eigenmodes with similar effective indices, $n_{eff} < n_{cl}$. These modes, by definition, do not satisfy the TIR condition, and hence are normally expected to have high confinement loss because they radiate away from the waveguide; hence they acquired the common nomenclature of "cutoff" or "leaky" modes (*7*). However, these properties have a strong dependence on mode symmetry. Fiber eigenmodes are quantized by two transverse indices: L, denoting the azimuthal index resulting in the mode carrying OAM, and a radial index, m (manifesting in oscillatory field amplitude in the radial direction). Including polarization [left- or right-handed circular polarization (LCP or RCP)] orthogonality, a given $|L|$ comprises four modes: a pair of spin-orbit aligned (SOa) modes ($+|L|$, LCP and $-|L|$, RCP) with n_{eff} slightly different from a pair of spin-orbit antialigned (SOaa) modes ($-|L|$, LCP and $+|L|$, RCP) (*8*). As Fig. 1A shows, the transverse momentum k_T is progressively more oriented in the azimuthal rather than the radial direction as $|L|$ increases. Because the "escape" rate of a mode tends to increase as k_T is progressively more radially oriented, it follows that the confinement loss of unbound, radiative modes decreases as the mode's azimuthal index increases.

A more rigorous illustration of topological confinement is obtained by considering the waveguide eigenvalue equation (*9*)

$$\frac{d^2F(r)}{dr^2} + \frac{1}{r}\frac{dF(r)}{dr} + \left[k_0^2\left(n^2(r) - \frac{L^2}{k_0^2 r^2}\right) - \beta^2\right]F(r) = 0 \quad (1)$$

where r is the radial coordinate, $F(r)$ is the radial amplitude of the electrical field, $n(r)$ is the refractive index profile of the fiber, $k_0 = 2\pi/\lambda$ is the free-space wave vector of light of wavelength λ, and β ($= k_0 \cdot n_{eff}$) is the propagation constant of an eigenmode. The attractive potential that enables TIR-induced bound modes is $n^2(r)$, but in the presence of OAM, a modified effective potential may be defined as

$$n^2_{centrifugal}(r) = n^2(r) - \frac{L^2}{k_0^2 r^2} \quad (2)$$

Figure 1B is a plot of this topologically modified profile, $n_{centrifugal}(r)$, experienced by cutoff modes with three nonzero L's, calculated at different wavelengths such that they have identical $n_{eff} < n_{cl}$. As is evident, cutoff modes encounter refractive index barriers (index trenches) of progressively greater magnitudes as $|L|$ increases. Hence, although the mode is no longer strictly bound by TIR (so that it no longer experiences zero confinement loss), its confinement loss strongly depends on $|L|$ because of the centrifugal barrier that light's OAM creates for itself.

Figure 1C shows the simulated confinement loss versus $|L|$ for modes with radial orders

[1]Boston University, Boston, MA 02215, USA. [2]OFS-Fitel, 2605 Brøndby, Denmark.
*Corresponding author. Email: sidr@bu.edu

Corrected 28 April 2023. See full text.

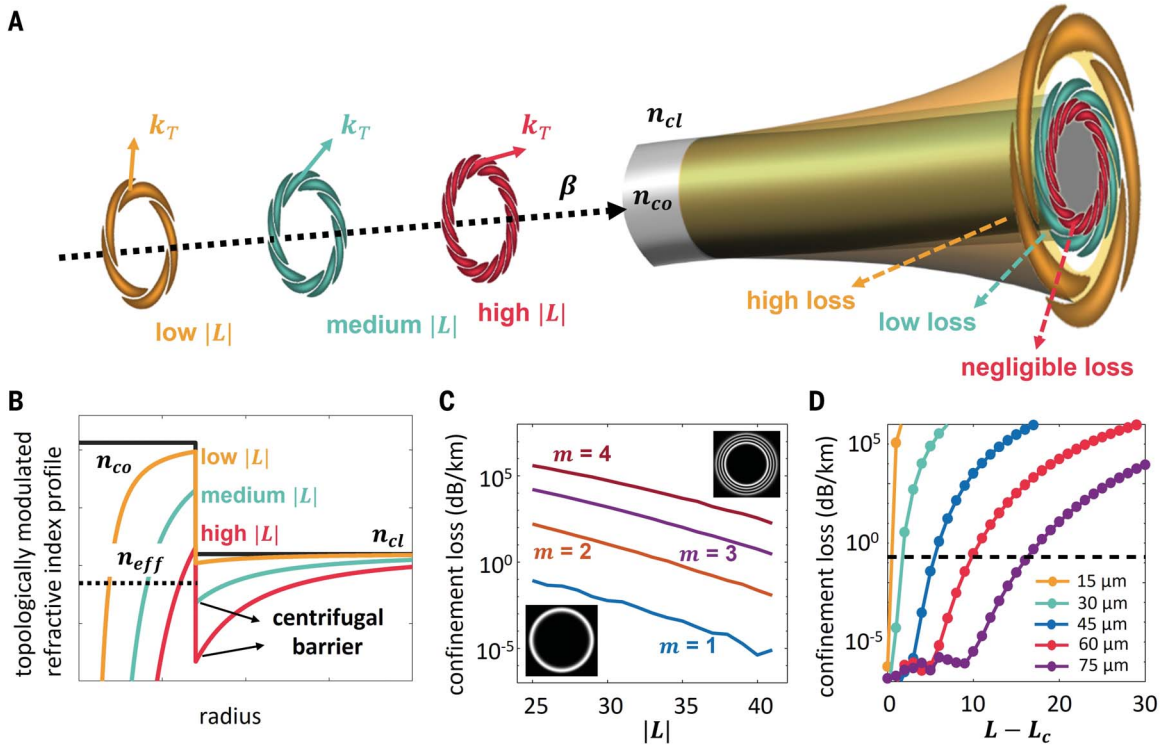

Fig. 1. The principle of light transport with TCMs. (**A**) The propagation of three cutoff OAM modes with different L's but identical n_{eff} in an exemplary step-index fiber. Select OAM modes in this fiber are illustrated as spiral patterns for visual clarity, with the number of spiral arms equal to $|L|$. Confinement loss of these modes decreases as $|L|$ increases because their transverse wave vectors, k_T, become progressively more azimuthally oriented. (**B**) Topologically modulated refractive index profile for the three cutoff OAM modes shown in (A). Higher $|L|$ induces a deeper index trench, creating a centrifugal barrier that prevents the cutoff modes from leaking out. (**C**) Simulated confinement loss versus mode orders L and m in a step-index fiber with 60-μm ring diameter. The n_{eff}'s of all the modes are held 1% below n_{cl}. Insets are simulated modal images of m = 1 and m = 4 modes. (**D**) Simulated confinement loss at 1550 nm versus relative OAM order $L - L_c$, in five step-index fibers with the same index contrast but different core sizes. L_c is the OAM order of the last TIR bound mode (L_c = 7, 16, 25, 35, and 45 for fiber core sizes of 15, 30, 45, 60, and 75 μm, respectively). Dashed line represents the overall measured loss (0.2 dB/km) of SMF-28.

$m \in [1,4]$ of a step-index fiber with $n_{co} - n_{cl}$ = 0.04 and core diameter of 60 μm, using a standard-perfectly-matched-layer model (*10*) (data points are simulated at different λ's such that n_{eff}/n_{cl} is identical for all modes). Modes of low $|L|$s, and modes of high m regardless of $|L|$, are highly lossy, justifying their long-hld nomenclature as "cutoff" or "leaky" modes, but for first radial order (m = 1) modes of sufficiently high $|L|$, confinement loss decreases substantially, down to as low as ~10^{-6} dB/km. Hence, although TCMs with high $|L|$ and m = 1 do not satisfy TIR, their confinement loss suggests that their behavior mirrors that of conventional TIR bound modes.

Figure 1D shows the simulated confinement loss versus relative topological charge ($L - L_c$, where L_c is the topological charge of the last bound mode, guided conventionally by TIR, before cutoff) at 1550 nm in five different step-index fibers of identical index contrasts (as in Fig. 1C), but with core diameters ranging from 15 to 75 μm. Also shown is the overall measured loss (~0.2 dB/km) for conventional transmission fibers (e.g., SMF-28). The number of modes that have confinement loss substantially lower than SMF-28 loss increases with $L - L_c$. This yields a crucial design criterion for realizing fibers that scale mode count with TCMs. Any fiber with a discrete index step at its outer core boundary (required for the existence of a centrifugal barrier; Fig. 1B) that guides, through conventional TIR, sufficiently high-$|L|$ modes (high L_c), has a large ensemble of even higher-$|L|$ cutoff modes that also experience negligible confinement loss, and the number of available TCMs simply increases with TIR bound-mode count. This rule implies that TCMs exist in any highly multimoded waveguide, comprising either high index contrasts, large core sizes, or both.

We tested this concept using a ring-core fiber with a ring outer diameter of 56.6 μm because it is functionally similar to a step-index fiber (fig. S1) (*11*–*13*). Figure 2A shows the cutback loss measurements on all SOa and SOaa modes with m = 1, $|L| \in [25,43]$. Conventional TIR bound modes have an average loss of ~1.4 dB/km, whereas TCM losses are ~5.1 dB/km (ignoring high-loss outliers that are not included in mode counts discussed in the next section). As is evident, TCM losses are orders of magnitude lower than conventional wisdom posits for cutoff modes, validating the idea that centrifugal barriers greatly aid light transmission for modes that are supposed to be radiated away. Barring a few transition TCMs that interact with parasitic high-m modes (fig. S4), the measured loss scales adiabatically, and only slightly, with mode order $|L|$. Moreover, we find that TCM losses decrease considerably with increasing fiber-draw tension (fig. S3). These findings suggest that interfacial scattering loss at the core-cladding boundary plays a dominant role in the loss measured in the current fiber (*14*, *15*), and that further glass viscosity and drawing-parameter optimizations promise substantially lower losses for TCMs. Given that simulated confinement losses for the TCMs (Fig. 2A, black dashed curve) are as low as ~10^{-6} dB/km, and that low-loss telecommunications-grade fibers with similar index contrasts and index gradients are regularly available (*16*), we expect manufacturing optimizations to substantially reduce TCM losses down to those of commercial high-index-contrast SMFs.

This topological effect is analogous to the OAM-dependent, above-threshold ionization of electrons in atomic orbitals (*17*) and to the metastability of Feshbach molecules in high rotational states (*18*). The effect is also well known in the context of nuclear reactions (*19*).

Corrected 28 April 2023. See full text.

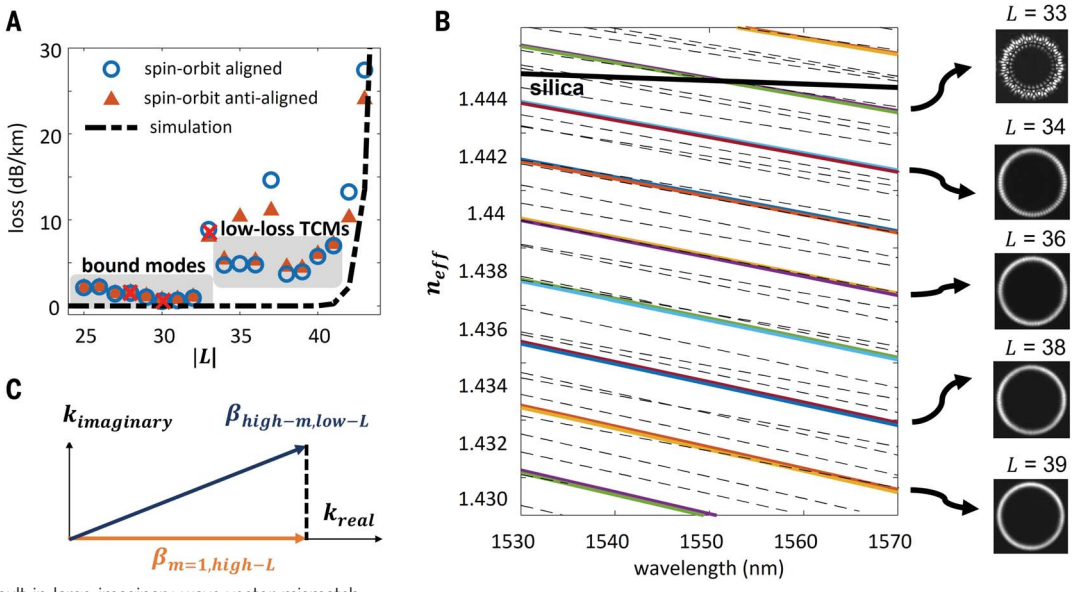

Fig. 2. Guidance beyond cutoff and natural distortion immunity of TCMs. (**A**) Experimental and simulated confinement loss at 1550 nm. (**B**) (Left) n_{eff} versus λ for select modes. Solid colored lines are desired m = 1 modes of different $|L|$; dashed black lines represent undesired high-m modes. The solid black line shows the index of the silica cladding (conventional boundary between TIR bound and cutoff modes). (Right) Experimentally measured output images of LCP modes at 1550 nm out of a 480-m-long ring-core fiber. (**C**) Schematic illustration of the mismatch between the complex β of desired m = 1 and undesired high-m cutoff modes, showing that coupling can be frustrated even when n_{eff} of modes match because their loss differences result in large imaginary wave-vector mismatch.

For light, centrifugal barriers increase the lifetimes of photons in whispering-gallery cavities (*20*, *21*).

Natural immunity to mode mixing

The key benefit of this regime of light transport is not just in the availability of more eigenstates—that result could potentially have been achieved with larger waveguides or higher-index cores for conventional TIR bound modes; rather, it is that topological confinement radically changes the density of states of low-loss propagating modes in multimode fibers, with implications for modal fidelity, as demonstrated below.

Figure 2B shows the simulated n_{eff} versus λ of select modes in the same ring-core fiber. Solid colored lines represent m = 1 modes of various $|L|$, and the dashed black lines represent high-m modes. It is immediately apparent that in a highly multimoded fiber, the different dispersion relationships for modes of different radial and azimuthal orders result in a plethora of degeneracies, making them especially susceptible to mode mixing. This is evident from a transmission experiment (fig. S2A) over a 480-m-long fiber, in which an attempt at sending a signal in a conventional TIR bound mode (L = 33, m = 1) results in a completely distorted output mode image (because it is uncontrollably coupled with the degenerate L = 16, m = 4 mode). Such modal degeneracies are the primary reason behind the current lack of progress in scaling cross-talk–minimized mode counts using conventional TIR bound modes.

By contrast, markedly distinct behavior is evident for TCMs (whose n_{eff} lie below the silica cladding index, depicted as a solid black curve in Fig. 2B). Although the L = 39, m = 1 mode is degenerate with an L = 24, m = 4 mode, the output image still shows a clear single ring. Modal degeneracy does not cause modal distortions in this case because the two modes have orders-of-magnitude-different confinement losses (Fig. 1C), leading to frustration of phase-matched coupling (*22*) (Fig. 2C). As such, all TCMs ($|L| \geq 34$, m = 1) show clean measured modal output images even though some transition TCMs reveal extra total loss (fig. S4). Hence, operation in the TCM regime allows scaling mode count while decreasing the modal density of states that cause unwanted perturbative mixing.

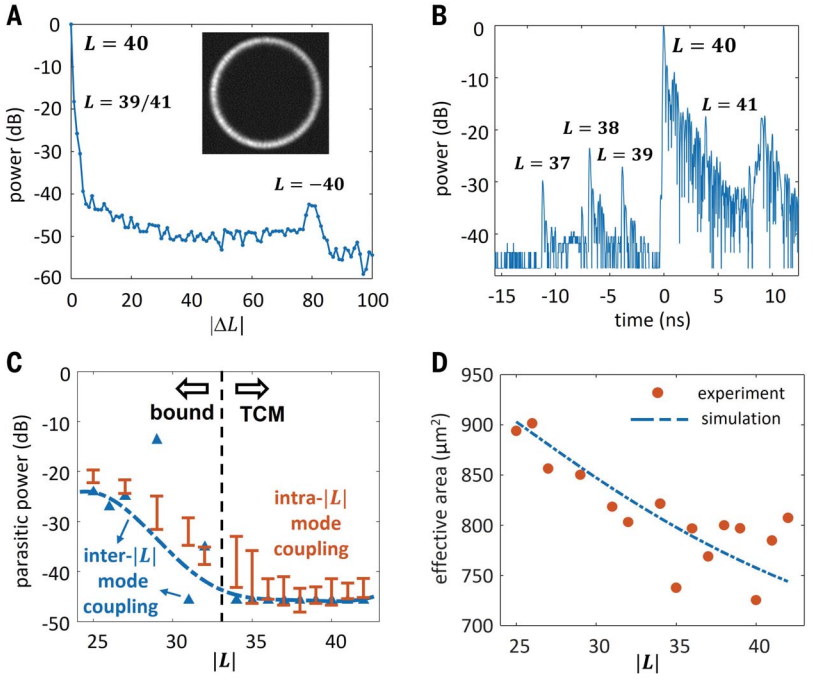

Fig. 3. Modal characterization of the TCM-supporting ring-core fiber at 1550 nm. (**A**) Parasitic mode power spectrum for L = 40, RCP launched mode measured by spatial interferometry. (Inset) Launched mode image at fiber output. (**B**) Time-of-flight trace of L = 40, RCP launched mode. (**C**) Parasitic power for inter-$|L|$ and intra-$|L|$ coupling. (**D**) Measured and simulated A_{eff} at 1550 nm versus $|L|$.

Fiber properties and transmission characteristics

We quantified the cross-talk of desired m = 1 modes at 1550 nm over this 480-m-long fiber using two techniques: (i) spatial interferometry (*23*), which yields power coupled in all modes for a given launched mode, and (ii) impulse-response measurements (*5*), which help disambiguate fundamental cross-talk due to in-fiber coupling from "technical," discrete cross-talk from multiplexers. The latter is of

Corrected 28 April 2023. See full text.

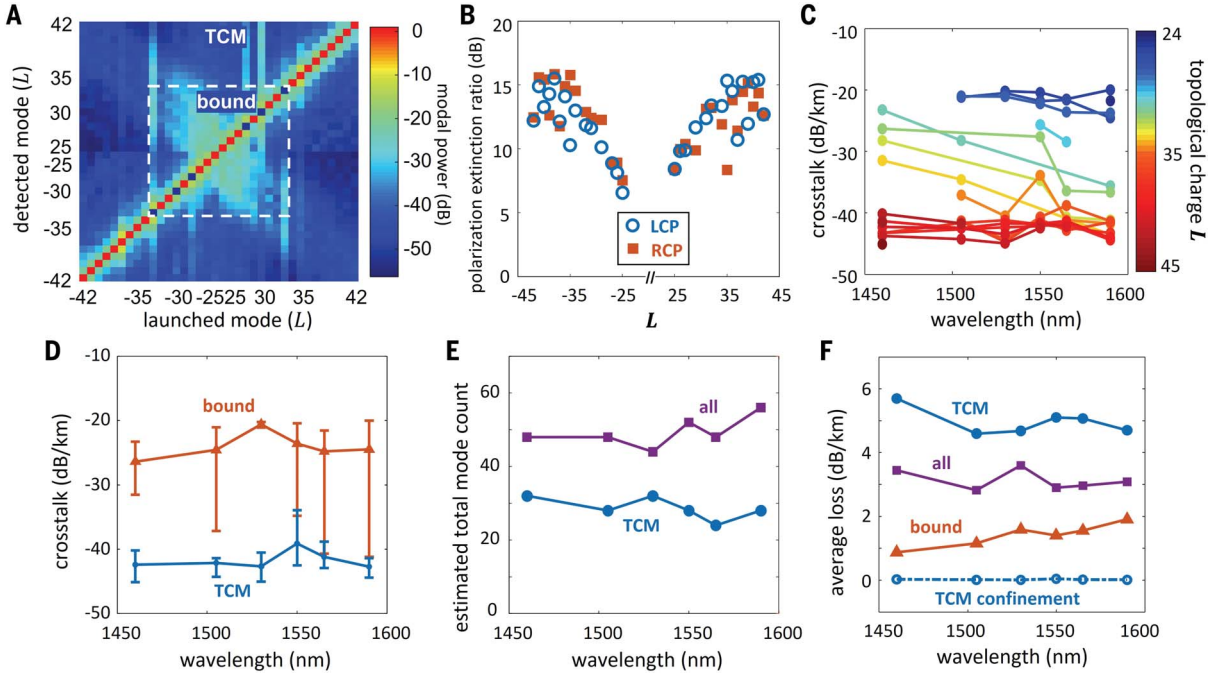

Fig. 4. Information capacity potential of TCM-supporting ring-core fibers. (**A**) Transfer matrices of all the modes with RCP. The red markers along diagonal indicate good modes; deep-blue markers indicate unstable, mixed modes. The box enclosed by the white dashed line denotes transition between TIR bound modes and TCMs. (**B**) PER of all available modes with LCP and RCP. (**C**) Cross-talk versus λ of modes with +|*L*|, RCP in S, C, and L telecommunications bands. (**D**) Cross-talk versus λ for TIR bound modes and TCMs. The color curves are the average cross-talk; error bars indicate the maximum and minimum values. (**E**) Estimated total mode count versus λ for TCMs and the sum of TCMs and TIR bound modes. (**F**) Average loss versus λ of good bound modes, TCMs, and their sum. The dashed curve represents the average simulated confinement loss of TCMs.

minimal concern in our analysis because it could be substantially minimized by using compact, fiber-compatible integrated mode transformers (*24*) in practical applications. Figure 3A shows an exemplary spatial interferometry measurement when the L = +40, RCP mode is launched. Parasitic power at the output primarily resides in two modes (supplementary text): in the L = −40, RCP mode at the −43-dB level, and in modes separated from the launched mode by ΔL = ±1, at the −20-dB level. The former (intra-|L| mode coupling) arises from in-fiber coupling between nearest neighbors (in n_{eff}), whereas the latter (inter-|L| mode coupling) arises from experimental mode-launch imperfections, as well as in-fiber, bend-induced coupling. A representative impulse-response measurement for the same launched mode reveals two distinct features of inter-|L| coupling: discrete coupling resulting in a spike in temporal trace that is due to mode launching, and distributed coupling between this spike from the L = 39 mode and the main peak for the L = 40 mode. The integrated power of this distributed coupling is found to be lower than the noise floor of the measurement (−46 dB). Figure 3C is concerned only with coupling of the fundamental (in-fiber, distributed) kind and plots the parasitic power of these two main sources of mode coupling for launched modes of interest in this fiber (supplementary text). The first finding of interest is that intra-|L| coupling dominates over bend-induced inter-|L| coupling, justifying using the intra-|L| coupling to represent the cross-talk (supplementary text). The second, more notable finding is that TCMs are more resistant to mode mixing, featuring cross-talk < −40 dB/km for almost all TCMs, barring a few outliers primarily at the transition between bound and cutoff modes. Some TCMs reach cross-talk as low as −45 dB/km. By contrast, the cross-talk for conventional TIR bound modes remains ~−20 dB/km, the same as that found in previous investigations of MMFs (*5*). Figure 3D shows that the effective areas (A_{eff}) of these modes, measured from recorded intensity profiles (*12*), are an order of magnitude larger than those for SMFs or MCFs. Furthermore, we find that all these attractive attributes of TCMs are maintained even when the fiber is bent down to radii as small as 6 mm (fig. S5).

To characterize this fiber over kilometer lengths of practical utility in data center applications, we used a Sagnac reflector to equivalently double the length of our 480-m-long fiber (*25*) (fig. S2B). Figure 4A shows the full transfer matrix for all the modes |L| = 25 – 42, RCP (Identical performance for LCP modes is shown in fig. S6.). Except for the outlier |L| = 28, 30, 33 modes (deep-blue square markers along the diagonal indicate TIR bound modes that experience mode mixing), and not counting the outliers in the TCM regime that exhibit high loss (Fig. 2A), we obtained 50 modes (red square markers) that exhibit cross-talk of ~−40 dB/km for TCMs and ~−20 dB/km for conventional TIR bound modes (based on measured power in the antidiagonals). The majority of the power in the two off-diagonals adjacent to the launched mode are from mode-launch imperfections, whereas fundamental in-fiber, bend-induced cross-talk in these modes is immeasurably low. We also measured the polarization extinction ratios (PER) (Fig. 4B) (*12*), which increased with |L| from ~10 to ~15 dB because of the fundamental property of OAM conservation (*26*). Figure 4C shows dominant (intra-|L|) in-fiber cross-talk for measurements repeated for λ ∈ [1460,1590] nm, covering the telecommunications S and C band and part of the L band (as before, outlier modes with excessive mode mixing or loss were excluded). Red and blue curves of various shades denote TCM and TIR bound-mode cross-talk, respectively. The cross-talk of modes depicted by other colors are typically for TIR bound modes that are close to cutoff, and hence modes that resemble TCMs as wavelength increases. Again, the average cross-talk of all TCMs lies between −40 and −45 dB/km, whereas most bound modes appear pinned at a cross-talk of −20 dB/km, regardless of wavelength. Especially apparent is the cross-talk

of TIR bound modes close to cutoff, demonstrating that, as the guidance mechanism for light evolves from TIR to topological confinement, the cross-talk also improves by two orders of magnitude. In addition, Fig. 4, D to F depicts the cross-talk, mode count, and average loss, respectively, demonstrating a 1-km-long MMF with record-high mode counts of ~50, comprising ~20 conventional TIR bound modes with < −20 dB/km cross-talk and ~30 TCMs with cross-talk < −40 dB/km across three telecommunications spectral bands of interest. The measured cross-talk and mode counts are on par with those of MCFs (*27*), and the broad bandwidth promises the compatibility with wavelength-division multiplexing. The 10× larger A_{eff} and chromatic dispersion (fig. S7C), as well as the relatively large differential modal delays (fig. S7, A and B), suggest that transmission in TCMs may be helpful in managing nonlinear signal distortions (*28*, *29*) in telecommunications applications. In addition, a plethora of low-cross-talk modes potentially enables low cross-talk per superpositions of modes as well (*30*), as required for quantum transport, effectively allowing high-dimensional encoding (*2*) and sources through intermodal interaction (*31*). Average losses for TCMs (~5.0 dB/km) and for TIR bound modes (~1.4 dB/km) are, at their current maturity, reasonable for amplifier and inter–data center applications, but because confinement losses are predicted to be much lower, manufacturing optimizations (fig. S3) would make these fibers suitable for substantially longer telecommunications links.

Summary and conclusions

The physics of frustrated coupling in TCMs yields an improvement of over two orders of magnitude in mode-coupling resistance over any MMF demonstrated to date. This fundamental feature has enabled cross-talk and channel counts that are on par with MCFs, while providing additional crucial benefits, such as order-of-magnitude-greater mode areas and extreme bend tolerance. By contrast, TCMs are propagating modes of an MMF, and as such, share other favorable attributes including high spatial efficiency and the prospect of efficient, gain-equalized optical amplification of all channels. Thus, topological confinement represents a regime of light transport that combines the benefits of both MCFs and conventional MMFs, yielding a platform that is not only suitable for scaling the capacity of classical telecommunications and quantum networks but also serves as a distinctive fiber-laser and nonlinear signal-processing medium on account of their large chromatic dispersions and record-large mode areas.

REFERENCES AND NOTES

1. P. J. Winzer, D. T. Neilson, *J. Lightwave Technol.* **35**, 1099–1115 (2017).
2. M. Erhard, M. Krenn, A. Zeilinger, *Nat. Rev. Phys.* **2**, 365–381 (2020).
3. B. J. Puttnam, G. Rademacher, R. S. Luís, *Optica* **8**, 1186–1203 (2021).
4. Y. Jung, S. Alam, D. J. Richardson, S. Ramachandran, K. S. Abedin, in *Optical Fiber Telecommunications VII*, A. E. Willner, Ed. (Academic Press, 2020), pp. 301–333.
5. P. Gregg, P. Kristensen, S. Ramachandran, *Opt. Express* **24**, 18938–18947 (2016).
6. Z. Ma, P. Kristensen, S. Ramachandran, in *2020 Conference on Lasers and Electro-Optics (CLEO)*, San Jose, CA, 10 to 15 May 2020, paper SF1P.2 (Optica Publishing Group, 2020).
7. R. Sammut, A. W. Snyder, *Appl. Opt.* **15**, 477–482 (1976).
8. Z. Ma, S. Ramachandran, *Nanophotonics* **10**, 209–224 (2020).
9. A. K. Ghatak, K. Thyagarajan, *Introduction to Fiber Optics* (Cambridge Univ. Press, 1998).
10. J. P. Berenger, *J. Comput. Phys.* **114**, 185–200 (1994).
11. Z. Ma, P. Kristensen, S. Ramachandran, in *2021 Conference on Lasers and Electro-Optics (CLEO)*, San Jose, CA, 9 to 14 May 2021, paper SM1F.4 (2021).
12. Materials and methods are available as supplementary materials.
13. Z. Ma, P. Kristensen, S. Ramachandran, in *2021 European Conference on Optical Communication (ECOC)*, Bordeaux, France, 13 to 16 September 2021, paper TU4A.3 (2021).
14. M. E. Lines, *J. Appl. Phys.* **55**, 4052–4057 (1984).
15. M. Wandel, "Attenuation in silica-based optical fibers," thesis, Technical Univ. of Denmark (2005).
16. M. Wandel, P. Kristensen, in *Fiber Based Dispersion Compensation*, S. Ramachandran, Ed. (Springer, 2007), pp. 7–42.
17. R. R. Freeman, P. H. Bucksbaum, *J. Phys. At. Mol. Opt. Phys.* **24**, 325–347 (1991).
18. C. Chin, R. Grimm, P. Julienne, E. Tiesinga, *Rev. Mod. Phys.* **82**, 1225–1286 (2010).
19. J. M. Blatt, V. F. Weisskopf, *Theoretical Nuclear Physics* (Wiley, 1952).
20. A. Chiasera *et al.*, *Laser Photonics Rev.* **4**, 457–482 (2010).
21. M. Sumetsky, *Phys. Rev. Lett.* **111**, 163901 (2013).
22. D. B. Stegall, T. Erdogan, *IEEE Photonics Technol. Lett.* **11**, 343–345 (1999).
23. N. Bozinovic, S. Golowich, P. Kristensen, S. Ramachandran, *Opt. Lett.* **37**, 2451–2453 (2012).
24. S. Bade *et al.*, in *Optical Fiber Communications Conference 2018 (OFC)*, San Diego, CA, 11 to 15 March 2018, paper Th4B.3 (Optica Publishing Group, 2018).
25. Z. Ma, M. W. Khalid, S. Ramachandran, in *2022 Conference on Lasers and Electro-Optics (CLEO)*, San Jose, CA, 15 to 20 May 2022, paper STu4P.3 (Optica Publishing Group, 2022).
26. P. Gregg, P. Kristensen, S. Ramachandran, *Optica* **2**, 267–270 (2015).
27. Y. Sasaki, in *2017 Optical Fiber Communications Conference (OFC)*, Los Angeles, CA, 19 to 23 March 2017, paper Th1H.2 (2017).
28. A. D. Ellis, N. Mac Suibhne, F. C. Gunning, S. Sygletos, *Opt. Express* **21**, 22834–22846 (2013).
29. G. Rademacher, K. Petermann, *J. Lightwave Technol.* **34**, 2280–2287 (2016).
30. A. P. Greenberg, G. Prabhakar, S. Ramachandran, *Nat. Commun.* **11**, 5257 (2020).
31. X. Liu, D. B. Kim, V. O. Lorenz, S. Ramachandran, in *Quantum 2.0*, Boston, MA, 13 to 16 June 2022, paper QTh4B.1 (Optica Publishing Group, 2022).

ACKNOWLEDGMENTS

We thank A. P. McCall and M. W. Khalid for help with instrumentation in the experiments. **Funding:** This study was supported by the Vannevar Bush Faculty Fellowship (N00014-19-1-2632), the Office of Naval Research (ONR) Multi University Research Initiative (MURI) (Grant N00014-20-1-2450), Brookhaven National Labs (Contract 354281), and the Air Force Office of Scientific Research (AFOSR) BRI program (Grant FA9550-14-1-0165). **Author contributions:** Conceptualization: Z.M. and S.R. Methodology: Z.M., P.K., and S.R. Investigation: Z.M. Visualization: Z.M. Funding acquisition: S.R. Project administration: S.R. Supervision: S.R. Writing – Z.M., P.K., and S.R. **Competing interests:** S.R. and Z.M. are inventors on a patent (US11506841B2) submitted by Boston University that covers the topological guidance of light described in this paper. P.K. declares no competing interests. **Data and materials availability:** All data are available in the main text or the supplementary materials.

SUPPLEMENTARY MATERIALS

science.org/doi/10.1126/science.add1874
Materials and Methods
Supplementary Text
Figs. S1 to S7
Reference (*32*)

Submitted 27 May 2022; resubmitted 23 December 2022
Accepted 22 March 2023
10.1126/science.add1874